The Astrophysical Journal, 713:637–650, 2010 April 10 doi:10.1088/0004-637X/713/1/637

THE FIRST MID-INFRARED VIEW OF THE STAR-FORMING PROPERTIES OF NEARBY GALAXY GROUPS

Lei Bai[1], Jesper Rasmussen[1,4], John S. Mulchaey[1], Ali Dariush[2], Somak Raychaudhury[3], and Trevor J. Ponman[3]
[1] The Observatories of the Carnegie Institution of Washington, 813 Santa Barbara Street, Pasadena, CA 91101, USA; leibai@obs.carnegiescience.edu
[2] Cardiff School of Physics and Astronomy, Cardiff University, Queens Buildings, The Parade, Cardiff CF24 3AA, UK
[3] School of Physics and Astronomy, University of Birmingham, Birmingham B15 2TT, UK
Received 2009 October 12; accepted 2010 March 1; published 2010 March 24

ABSTRACT

We present the first mid-IR study of galaxy groups in the nearby universe based on *Spitzer* MIPS observations of a sample of nine redshift-selected groups from the *XMM*-IMACS project, at $z = 0.06$. We find that on average the star-forming (SF) galaxy fraction in the groups is about 30% lower than the value in the field and 30% higher than in clusters. The SF fractions do not show any systematic dependence on group velocity dispersion, total stellar mass, or the presence of an X-ray emitting intragroup medium, but a weak anti-correlation is seen between SF fraction and projected galaxy density. However, even in the densest regions, the SF fraction in groups is still higher than that in cluster outskirts, suggesting that preprocessing of galaxies in group environments is not sufficient to explain the much lower SF fraction in clusters. The typical specific star formation rates (SFRs/M_*) of SF galaxies in groups are similar to those in the field across a wide range of stellar mass ($M_* > 10^{9.6}\,M_\odot$), favoring a quickly acting mechanism that suppresses star formation to explain the overall smaller fraction of SF galaxies in groups. If galaxy–galaxy interactions are responsible, then the extremely low starburst galaxy fraction (<1%) implies a short timescale (∼0.1 Gyr) for any merger-induced starburst stage. Comparison to two rich clusters shows that clusters contain a population of massive SF galaxies with very low SFR (14% of all the galaxies with $M_* > 10^{10}\,M_\odot$), possibly as a consequence of ram pressure stripping being less efficient in removing gas from more massive galaxies.

Key words: galaxies: clusters: general – galaxies: evolution – infrared: galaxies

1. INTRODUCTION

The local galaxy population presents a clear bimodality in many different properties: blue galaxies with active star formation and late-type morphologies versus red, quiescent galaxies with early-type morphologies (e.g., Strateva et al. 2001; Baldry et al. 2004; Balogh et al. 2004). This bimodality is ubiquitous, extending from galaxy clusters to groups and to the general field (Lewis et al. 2002; Gómez et al. 2003). The physical origin of this bimodality remains one of the most puzzling questions of galaxy formation and evolution. Is the difference of the two distinct populations seeded in the early stages of galaxy formation (the so-called nature scenario), or is it the end result of a transformation driven by environment (the "nurture" scenario)? Strong evidence favoring the nurture scenario comes from the drastic change of the fraction of galaxies in these two populations in different environments: the fraction of passive galaxies increases with increasing galaxy density. However, such a correlation alone does not directly imply a nurture scenario. The fraction of galaxies in different populations also depends on galaxy stellar mass (Kauffmann et al. 2003), which could have a different distribution in low- and high-density regions seeded at the time of galaxy formation. Hence, to fully understand galaxy evolution, we need to disentangle the stellar mass and environment dependence (e.g., Baldry et al. 2006; Iovino et al. 2010; Kovac et al. 2009) and identify the mechanisms responsible for establishing the bimodality in galaxy properties.

Galaxy groups, as the most common galaxy associations, contain about 50% of the galaxy population at the present day (Geller & Huchra 1983; Tully 1987; Eke et al. 2004, 2005). The characteristic depth of the potential wells of groups is similar to those of individual galaxies, and the velocities of galaxies within groups are only a few hundred km s^{-1}, comparable to the internal velocity of galaxies. Under these circumstances, galaxies interact strongly with one another, and with the group as a whole. Such interactions could transform the morphology of galaxies, induce starbursts, and thereby turn active, late-type galaxies into quiescent, early-type galaxies. In addition, the group environment could also transform galaxies via ram pressure stripping of their hot gas halos, eventually suffocating star formation (Rasmussen et al. 2006a; Kawata & Mulchaey 2008; McCarthy et al. 2008). Hence, not only are groups the most common environmental phase experienced by galaxies during their evolution, they also have the potential to strongly affect large populations of galaxies and thereby help to explain the ubiquitous bimodality in galaxy properties.

Another important implication of galaxy transformations in groups is the preprocessing of galaxies before they fall into clusters (Zabludoff & Mulchaey 1998). In a hierarchical structure formation scenario, clusters are built up by the accretion of smaller structures, e.g., isolated galaxies and groups. However, it is still under debate if the majority of cluster galaxies were ever located in groups before being acquired by clusters (Berrier et al. 2009; McGee et al. 2009). If the fraction of cluster galaxies accreted in groups is substantial, preprocessing of galaxy properties by the group environment could play a major role in forming the predominantly passive population in clusters. Additional physical mechanisms which only work efficiently in the cluster environment, such as galaxy harassment and ram pressure stripping of cold galactic gas, could further affect galaxy properties but would possibly only be of secondary importance.

Despite the importance of the group environment for the global galaxy population, our understanding of groups is still very limited. There have been many studies of group galaxies trying to address these questions. Due to the low galaxy density contrast against the field, many previous group studies

[4] *Chandra* Fellow.

focused on X-ray luminous groups, which are mostly virialized groups (Mulchaey & Zabludoff 1998; Zabludoff & Mulchaey 1998). However, when referring to the majority of galaxies as being located in groups, this applies specifically to *optically* selected groups, typically identified through a "friends-of-friends" analysis of galaxy redshift survey data (Eke et al. 2004; Balogh et al. 2004). Such groups span a wide range of evolutionary states, including systems in the process of collapsing (like the Local Group), systems in the throes of strong galaxy interactions or subgroup mergers, and fully virialized systems. To fully assess the importance of the group environment on galaxy evolution, complete samples of galaxy groups extending to poor systems are essential. There have also been studies of optically selected groups based on large-area galaxy surveys (Balogh et al. 2004; Weinmann et al. 2006). However, due to the limited survey depth, many of the poor groups in those studies only contain a handful of known group members. To fully understand the dynamics and galaxy content of each group, we need to probe to significantly fainter optical magnitudes than is usually possible with such large surveys.

For this purpose, we have started the *XMM*-IMACS (XI) Groups Project (Rasmussen et al. 2006b, hereafter Paper I) to carry out a multi-wavelength study of a statistically representative nearby group sample. We selected 25 groups with velocity dispersion $\sigma < 500$ km s^{-1} from the group catalog of Merchán & Zandivarez (2002), which was carefully derived from a friends-of-friends analysis of the 2dF redshift survey (Colless et al. 2001). The groups are selected in a narrow redshift range ($0.06 < z < 0.062$) to minimize the redshift dependence of group properties. To fully represent the poor group population, the XI group sample was selected to span a wide range in group properties, e.g., velocity dispersion, virial radius, and number of group members (Rasmussen et al. 2006b). To extract membership information down to faint magnitudes, multislit spectroscopy of these groups has been performed using IMACS on the 6.5 m Baade/Magellan telescope (Bigelow & Dressler 2003), and for nine of the groups we have also obtained X-ray observations using *XMM-Newton*. At the chosen group redshifts, the fields of view of both IMACS and *XMM-Newton* cover the typical virial radius of the groups, ∼1 Mpc.

To assess the star formation properties of galaxies in these groups, we carried out *Spitzer* MIPS 24 μm imaging of the XI group sample. Different from emission line or UV luminosity often used in previous group studies to measure the star formation rate (SFR) of galaxies, the mid-IR emission from the dust heated by a young stellar population is a robust star formation indicator unaffected by extinction. Thus, IR emission is not only critical in giving us an unbiased view of the star formation properties of the group population, but more importantly, is essential to identify dusty starbursts in which the majority of the star formation is obscured and not seen in optical spectra (Liu & Kennicutt 1995). Although there have been many studies of star-forming (SF) galaxies using IR observations in clusters (Fadda et al. 2008; Geach et al. 2006; Marcillac et al. 2007; Bai et al. 2006, 2007, 2009; Dressler et al. 2009; Saintonge et al. 2008; Haines et al. 2009a, 2009b; Wolf et al. 2009; Mahajan & Raychaudhury 2009), such studies of groups have been lacking. While Tran et al. (2009) detected an excess of 24 μm SF galaxies in groups compared to the field, we note that their sample represents a somewhat peculiar case of a super-group in the process of forming a massive cluster.

In this paper, we present the first IR study of star formation in a representative, nearby sample of groups, based on nine groups in our XI sample. These are the first nine groups for which we have complete spectroscopic data and X-ray observations. We analyze the SF properties of group galaxies from their 24 μm emission and compare them to those of field and cluster galaxies. In Section 2, we describe the observations and data reduction, and in Section 3 discuss the general properties of the groups. In Section 4, we present the SF galaxy fractions and specific SFRs of group galaxies, and compare them to results for galaxies in clusters and the field. The results are discussed in Section 5 and summarized in Section 6. Throughout this paper, we assume a ΛCDM cosmology with parameter set $(h, \Omega_0, \Lambda_0) = (0.7, 0.3, 0.7)$.

2. OBSERVATIONS AND DATA

2.1. XI Groups

2.1.1. Optical Imaging and Spectroscopy

Optical images of the groups were taken in the Bessel *BVR* filters with the Wide Field Reimaging CCD (WFCCD) on the 100 inch du Pont telescope at Las Campanas. Source extraction and photometry were done with SExtractor (Bertin & Arnouts 1996). The magnitudes were corrected for Galactic extinction using the dust map from Schlegel et al. (1998). Follow-up multi-object spectroscopy of galaxies in the group fields was obtained with the IMACS spectrograph on the Baade/Magellan telescope. The spectra were taken with the 300 lines mm^{-1} prism on the $f/2$ camera, which covers a wavelength range of 3900–10000 Å at a dispersion of 1.34 Å pixel^{-1}. Spectroscopic targets were selected based on *R*-band magnitudes, prioritizing the brighter sources. The spectra were reduced using the COSMOS software package. We refer readers to Paper I for more details on the target selection, observing strategy, and data reduction. The redshifts of the galaxies were determined by cross-correlating with SDSS galaxy templates. Typical errors in the redshift measurements were ∼50 km s^{-1}.

In most group fields, our optical imaging and spectroscopy only cover the central $20' \times 20'$ region, which corresponds to 1.4×1.4 Mpc^2 at the relevant redshifts. To extend the spatial coverage to larger radii and better match the larger extent of the IR data, our spectroscopic data were complemented with redshift measurements from the NASA/IPAC Extragalactic Database (NED) and the 6dF Galaxy Survey (6dFGS; Jones et al. 2009). Most of the redshift measurements in NED are from 2dFGRS, which probes down to a magnitude limit of $b_J \leqslant 19.45$, while the 6dFGS extends down to $b_J \leqslant 16.75$. Some of those galaxies are outside the region covered by our imaging data. For these galaxies, we obtained *R*-band magnitudes from the SuperCOSMOS Sky Surveys (SSSs; Hambly et al. 2001), which are, where they overlap, consistent with the photometry derived from our imaging data. Our final spectroscopic catalogs are >80% complete down to $R = 18$ in the central $<10'$ (0.7 Mpc) region and >50% complete out to a radius of $25'$ (1.7 Mpc).

2.1.2. X-ray Observations

All nine groups discussed in this paper were observed by *XMM-Newton*. The details of the X-ray observations and analysis can be found in Paper I and Shen et al. (2007). The nominal exposure time in all fields is ∼20 ks, although the useful exposure time varies due to the presence of background flares in several of the observations. The typical detection limit for X-ray point sources is $\sim 2 \times 10^{40}$ erg s^{-1} (0.3–2 keV), assuming a power-law spectrum of photon index of 1.7 subject to Galactic

absorption. Extended emission from a hot intragroup medium is clearly detected in three groups, MZ 10451, MZ 4577, and MZ 9014. MZ 10451 is the most X-ray luminous group in our sample and has $L_X \sim 2 \times 10^{42}$ erg s^{-1} (Rasmussen et al. 2010), comparable to typical X-ray-selected groups with similar velocity dispersion. Both MZ 4577 and MZ 9014 have low levels of extended emission ($L_X \sim 10^{41}$ erg s^{-1}; Rasmussen et al. 2006b). A more detailed analysis of the *XMM-Newton* data will be presented in a future paper.

2.1.3. MIPS 24 μm Imaging and SFR Estimation

The 24 μm images of the groups were taken by MIPS (Rieke et al. 2004) on *Spitzer* in the medium scan map mode during 2007–2008. The observed field for each group was a rectangular region about $20' \times 45'$ (1.4×3.1 Mpc^2) in size centered at the group center from the Merchán & Zandivarez (2002, hereafter MZ) catalog. The data were processed with the MIPS Data Analysis Tool (DAT ver. 3.02; Gordon et al. 2005), and array-averaged background subtraction was applied to improve the signal-to-noise ratio. The final mosaics have an exposure time of ~80 s pixel^{-1} and a spatial resolution of ~5″. We used SExtractor to extract sources and measure their 24 μm flux within an adaptive Kron aperture (`flux_auto`). The sensitivity of the data varies slightly from field to field depending on the IR background level, but the 3σ point source detection limit is $\leqslant$0.35 mJy in all fields.

We correlated galaxies with the nearest 24 μm sources projected within 5″. This matching radius takes into consideration the possible physical displacement between the optical and 24 μm brightness centroids. To determine the SFR from the 24 μm flux, we use the conversion given by Rieke et al. (2009). However, the IR luminosity limit of our data, $\log L_{\rm IR}/L_\odot = 8.9$, is fainter than the lower limit to which this formula is applicable ($\log L_{\rm IR}/L_\odot = 9.7$). For galaxies with lower IR luminosity, the ratio of escaping UV photons to UV photons absorbed by dust increases (Buat et al. 2007). At $\log L_{\rm IR}/L_\odot \approx 11$, the average leakage is only about 2.5%, and this is the correction factor adopted by Rieke et al. (2009) in the derivation of their conversion formula. However, for less luminous galaxies, this correction is insufficient, as the average leakage increases to about 50% at $\log L_{\rm IR}/L_\odot = 8.5$ (Buat et al. 2007). To extend the SFR conversion to less luminous galaxies ($\log L_{\rm IR}/L_\odot < 11$), instead of using an average leakage fraction of 2.5%, we estimate the leakage as a function of $L_{\rm IR}$ using the average $L_{\rm IR}/L_{\rm UV}$ versus $L_{\rm bol}$ relation provided by Buat et al. (2007, their Figure 7), where $L_{\rm bol} = L_{\rm UV} + 0.7L_{\rm IR}$. We then correct the SFR derived from Rieke's formula with this leakage fraction. This correction is generally small, increasing the derived SFR at most by a factor of 2, and it only affects galaxies with low SFRs. With this conversion, the 24 μm detection limit of our observations translates into an SFR limit of 0.1 $M_\odot$ yr^{-1}.

In this work, we assume that the 24 μm emission of galaxies is predominantly from dust heated by young stars. This is true for SF galaxies and H II regions, based on which the 24 μm to SFR conversion is calibrated (e.g., Rieke et al. 2009). However, for galaxies with small 24 μm luminosities, especially early-type galaxies, the contribution from cold dust heated by an evolved stellar population becomes significant. Temi et al. (2009a, 2009b) have shown that for elliptical galaxies there is a correlation between 24 μm luminosity and the near-IR luminosity L_{K_s}, consistent with the expectation of mid-IR emission originating from cold dust surrounding the old, mass-losing red-giant stars. With this correlation, we can estimate the cold dust contribution to the 24 μm emission from L_{K_s}. To do so, we retrieved K_s-band luminosities of our group galaxies from the Two Micron All Sky Survey (2MASS), which is complete down to $R \sim 16$ at the group redshift. For group galaxies too faint to be detected by 2MASS, we estimate their K_s luminosity from R magnitudes. This introduces an extra uncertainty in our estimates, but for these less massive galaxies, the cold dust contribution is generally minimal compared to the 24 μm detection limit to which we are sensitive. Following Temi et al. (2009a), we regard the 24 μm emission of all galaxies with $\log (L_{24}/L_{K_s}) < 30.5$ (with L_{24} in erg s^{-1} and L_{K_s} in $L_\odot$) as coming exclusively from cold dust, setting their SFR to zero; for galaxies above this limit, we subtract a cold dust contribution, $\log L_{24,\rm cold} = (1.01 \pm 0.05) \log L_{K_s} + 30.1 \pm 0.5$, from the observed L_{24} before converting the latter into an SFR estimate. Overall, this cold dust correction for our sample is very small: for the 24 μm detected galaxies in our groups, none has L_{24} consistent with being from cold dust alone, and the majority has a cold dust contribution less than 10%.

Another complication of using mid-IR emission to derive SFR is the contamination from active galactic nucleus (AGN) activity. In this case, the dust is, at least partly, heated by AGNs and the correlation between SFRs and 24 μm flux no longer holds. To identify AGN, we cross-match group members with the X-ray point sources detected in each field. Using a matching radius of 10″, we found unambiguous X-ray counterparts, with $L_X > 10^{41}$ erg s^{-1}, for five galaxies in the nine groups. If we only consider the galaxies with $M_R < -20$ within the *XMM* field of view, the fraction of group galaxies with $L_X > 10^{41}$ erg s^{-1} is 6^{+12}_{-6}%, consistent with the 5% found in clusters (Martini et al. 2006). Of those five X-ray bright galaxies, only two are also detected at 24 μm. This only accounts for a small fraction (~2%) of the IR-detected galaxies. This fraction is also consistent with the result found in the A901/902 supercluster (Gallazzi et al. 2009). In addition to X-ray luminous AGN, Shen et al. (2007) also identified five optical AGN with no X-ray counterpart within our groups. All of these are bright at 24 μm. Even though these galaxies show emission line ratios typical of AGN, their IR emission is probably still dominated by star formation (e.g., Brand et al. 2009).

Because of the difficulty in removing the AGN contribution to the IR emission, and the small number of group galaxies with known AGN signatures, we do not exclude these AGN in our IR-selected SF galaxy sample. In the following sections, we compare our group SF galaxies to field and cluster SF galaxies and we note that these comparison samples of IR-selected SF galaxies may also be contaminated by AGN. However, the inferred dependence of AGN fraction on environment is generally weak (Kauffmann et al. 2004; Martini et al. 2006). In particular, the results of Shen et al. (2007) show that, down to the limiting magnitude of $M_R = -20$ that we consider for SF galaxies in Sections 4 and 5, the overall AGN fraction within our groups is consistent with that of rich clusters. Hence, we do not expect environmental differences in AGN activity to have a significant impact on our results.

2.2. Field and Cluster Comparison Samples

We further compiled a field galaxy sample from 23 XI group fields with MIPS data. For each field, we retrieved all the galaxies with redshifts from NED, where most of them are from the 2dFGRS survey. The redshift histogram of each field was examined to exclude foreground/background clusters and groups, resulting in a field sample of 77 galaxies in the redshift

Table 1
Individual Group Properties

Group	R.A.[a] (J2000)	Decl.[a] (J2000)	N[b]	$N_{\rm IMACS}$[c]	z[d]	σ[e] (km s^{-1})
MZ 10451	02:29:13.17	−29:38:58.1	60	34	0.06065	503^{+56}_{-71}
MZ 3849	10:27:49.26	−03:18:25.4	20	15	0.06054	298^{+30}_{-42}
MZ 4577	11:32:43.87	−03:57:55.7	35	17	0.06201	247^{+35}_{-41}
MZ 4592	11:30:46.48	−03:47:56.2	27	16	0.06162	215^{+23}_{-36}
MZ 4940	11:35:58.66	−03:41:05.0	12	8	0.06212	104^{+31}_{-58}
MZ 5293	12:16:25.78	−03:24:25.9	10	9	0.06204	99^{+11}_{-24}
MZ 5383	12:35:01.07	−03:36:11.3	47	25	0.06044	521^{+54}_{-63}
MZ 9014	00:38:05.40	−27:23:53.9	34	23	0.06094	322^{+30}_{-40}
MZ 9307	00:40:20.57	−27:32:17.7	28	16	0.05999	431^{+44}_{-72}

Notes.
[a] Coordinates of the luminosity-weighted group centers.
[b] Total number of group members.
[c] Number of group members with new redshifts measured by IMACS.
[d] Biweight mean redshift of group members.
[e] Velocity dispersion.

range of $0.02 < z < 0.57$. The R-band magnitudes of these galaxies were obtained from the 2dFGRS photometric catalog. Among these field galaxies, 45 are brighter than $M_R = -19$.

For comparison, we also compiled a cluster galaxy sample from two local rich clusters: the Coma cluster ($z = 0.023$) and the Abell 3266 cluster (A3266; $z = 0.06$). Both clusters have been observed with MIPS at 24 μm to similar depth as the XI groups. More details on the MIPS data of these two clusters are reported in Bai et al. (2006, 2009). Altogether, we have around 600 cluster galaxies with $M_R < -19$. We updated the 24 μm SFR conversion for these galaxies with the new method described in Section 2.1.3. Compared to the group and field galaxies, the cold dust correction is more important for cluster galaxies. About 20% of the cluster members have a cold dust contribution of more than 20%, and about 10% have a 24 μm flux consistent with being from cold dust alone.

3. GENERAL PROPERTIES OF THE GROUPS

3.1. Group Member Selection

To select group members, we performed an iterative 3σ clipping in redshift space using the biweight mean and dispersion (Beers et al. 1990) until the number of group members converged. In most groups, all galaxies with velocity ± 2000 km s^{-1} within the group mean and within 25′ (∼1.7 Mpc) of the group centers were included in the calculation. For MZ 3849 and MZ 9307, narrower velocity ranges were employed (1300 and 1500 km s^{-1}, respectively), in order to exclude contamination from nearby unrelated structures. In all cases, the calculations converged in one or two iterations. In total, we identified 273 group members in the nine groups. With the new membership lists, we updated the group redshifts and velocity dispersions, as listed in Table 1. The 1σ errors on the velocity dispersions were derived from bootstrap calculations. The velocity dispersions of our group sample range from ∼100 to 500 km s^{-1}. We also calculated the velocity dispersions using only galaxies within 1 Mpc from the group centers, confirming that the differences in resulting velocity dispersions are well within the estimated errors.

The galaxy velocity histogram in each field is plotted in Figure 1 in bins of 150 km s^{-1}, with group members indicated by the shaded area. In all cases, the group members form distinctive peaks in velocity space. Several groups show multiple peaks, suggesting possible substructure. In particular, the two richest groups, MZ 10451 and MZ 5383, both show two separate peaks. However, the projected galaxy distribution shows no obvious spatial segregation associated with these individual peaks to directly support the existence of substructure. Recently, Hou et al. (2009) concluded that the Anderson–Darling (A–D) test is a reliable tool to detect departures from a Gaussian velocity distribution in small data sets with size typical of our groups. Because a non-Gaussian velocity distribution could suggest an unrelaxed dynamical status, we performed the A–D test on our groups and found that the null hypothesis of a Gaussian distribution is rejected in the two richest groups at the 90% confidence level. This suggests that these two groups are not relaxed systems. For the rest of the groups, the A–D test does not reject the hypothesis of a Gaussian distribution. However, the power of the A–D test decreases in poorer systems (Hou et al. 2009), and consistency with a Gaussian velocity distribution need not imply a dynamically relaxed systems in such cases.

3.2. Morphology of the Groups

In Figure 2, we show the projected spatial distribution of the group members. Each plot is 1 deg × 1 deg in size, and the dotted rectangular region indicates the MIPS 24 μm coverage. It is clear from the plot that the galaxy distribution in several groups is rather irregular, with some of the groups showing evidence of substructure. Rich systems such as MZ 10451 and MZ 5383 tend to show clear concentrations in the galaxy distribution, whereas several of the poorer ones display a more filamentary overall morphology. However, the large uncertainty in determining the geometry of the galaxy distribution in poor systems renders such differentiation tentative at best. Furthermore, even the richer systems show evidence of prominent subclumps and elongated structures. We defer a detailed morphological analysis to a future paper, when spectroscopic results for the full XI group sample are available.

To determine the group center, we first calculated the R-band luminosity-weighted center including all the group members. We then exclude galaxies with velocities more than 2σ away from the cluster mean or projected distance larger than 15′ (∼1 Mpc) from the initial group center and recalculate the luminosity-weighted center. We plot these centers as green plus signs in Figure 2. We also overlay the luminosity-weighted galaxy surface density maps in the same plot. In many groups, as shown in the plot, the luminosity-weighted group centers are quite far away from the peak of the luminosity-weighted density map. In the three groups with clearly detected extended X-ray emission, MZ 10451, MZ 4577, and MZ 9014, the X-ray centroids are located closer to the galaxy density peak (<300 kpc) than to the luminosity-weighted group centers. These large displacements may suggest that these systems are still in the process of virialization. Throughout this paper, we use luminosity-weighted group centers as the group centers. However, we note that using luminosity-weighted galaxy density peaks (or X-ray centroids, where available) as the group centers do not change the general results in this paper.

Further evidence that many of these systems have not reached a fully virialized stage is the lack of a central brightest group galaxy (BGG). Nearby X-ray-selected groups generally have early-type BGGs sitting at the center of the group potential (Zabludoff & Mulchaey 1998; Mulchaey & Zabludoff 1998; Helsdon & Ponman 2000). In most of our groups, the brightest galaxies within 1 Mpc of the luminosity-weighted group centers

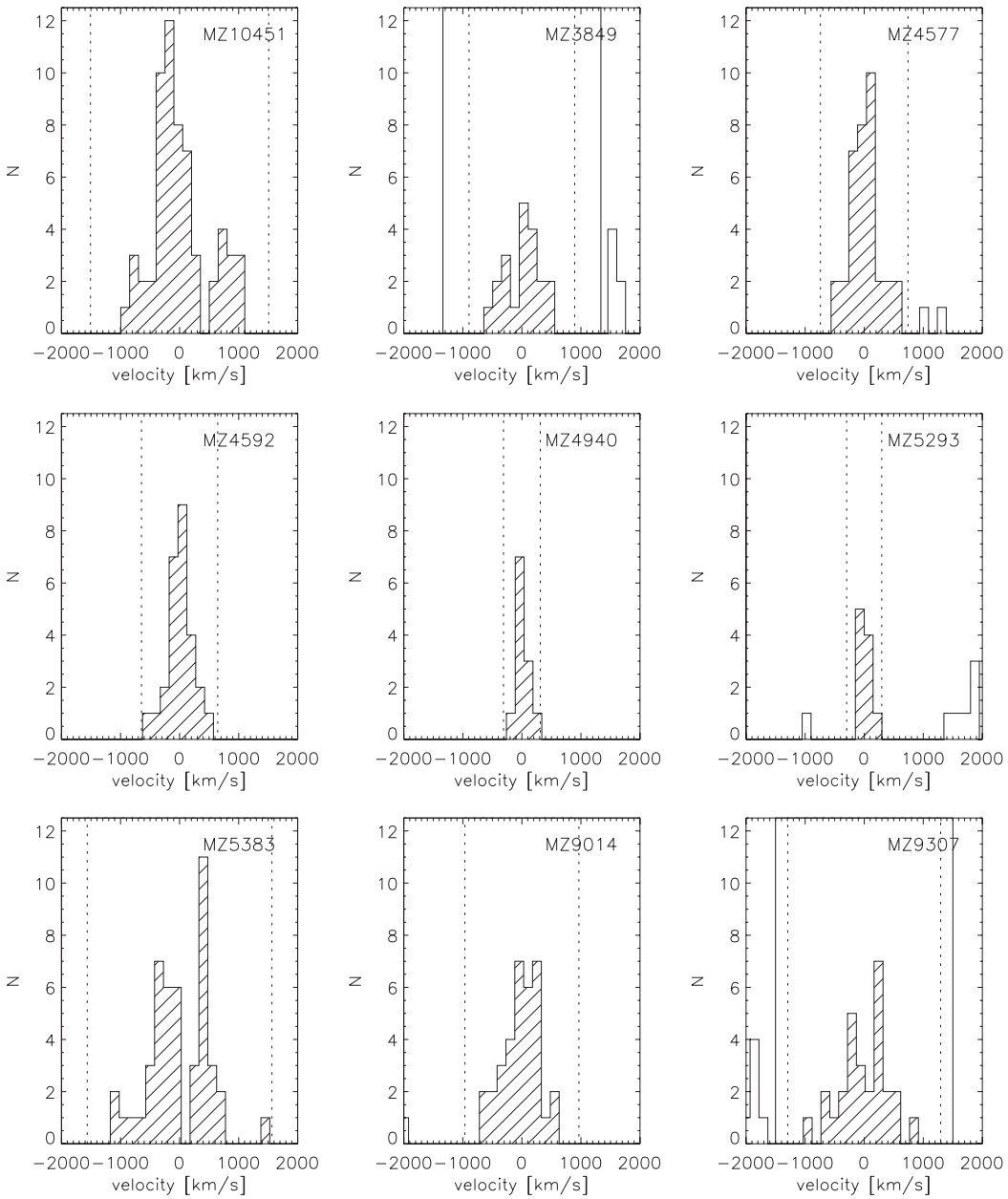

Figure 1. Galaxy velocity histograms of the groups. Shaded regions represent identified group members. Dotted vertical lines indicate the $\pm 3\sigma$ range. Solid vertical lines for MZ 3849 and MZ 9307 show the imposed velocity cuts needed to exclude nearby contamination. In other groups, this velocity cut is ± 2000 km s^{-1}.

are located >300 kpc away from the centers. Also, as shown in Figure 2, many of these BGGs are not coincident with the most crowded region in the groups. In the most X-ray luminous group in the sample, MZ 10451, the galaxy residing at the center of the X-ray emission is only the fourth brightest galaxy in the group. The BGG lies about 700 kpc away from the luminosity-weighted center and is about 1.2 Mpc away from the center of the X-ray emission, placing it beyond the virial radius according to the mass profile determined from our X-ray data (Rasmussen et al. 2010). In addition, it has a radial velocity of $\sim$1000 km s^{-1} relative to the group mean and is a spiral galaxy. These pieces of evidence strongly argue that this BGG is just a recently accreted galaxy. Moreover, the distribution of most of the bright galaxies in these groups is fairly scattered instead of being centrally concentrated, also suggestive of the systems generally not being dynamically old.

4. STAR-FORMING PROPERTIES OF THE GALAXIES IN XI GROUPS

4.1. Star-forming Galaxy Fractions

A statistical indicator of star formation activity in a galaxy population is the fraction of SF galaxies. The sensitivity of the 24 μm observations of the XI groups allows the detection of SF galaxies with SFR $> 0.1\,M_{\odot}\,\mathrm{yr}^{-1}$. We can therefore calculate the fraction of SF galaxies with SFR $> 0.1\,M_{\odot}\,\mathrm{yr}^{-1}$ for all the galaxies brighter than $M_R = -20$. We limit the SF fraction calculation to galaxies with $M_R \leqslant -20$, because the comparison cluster and field samples discussed in the following sections are only complete down to this limit. However, for the group galaxies, we confirmed that extending the fraction calculation to a fainter magnitude ($M_R \leqslant -19$) lowers the overall fractions but does not change any of our conclusions. Dwarf galaxies fainter

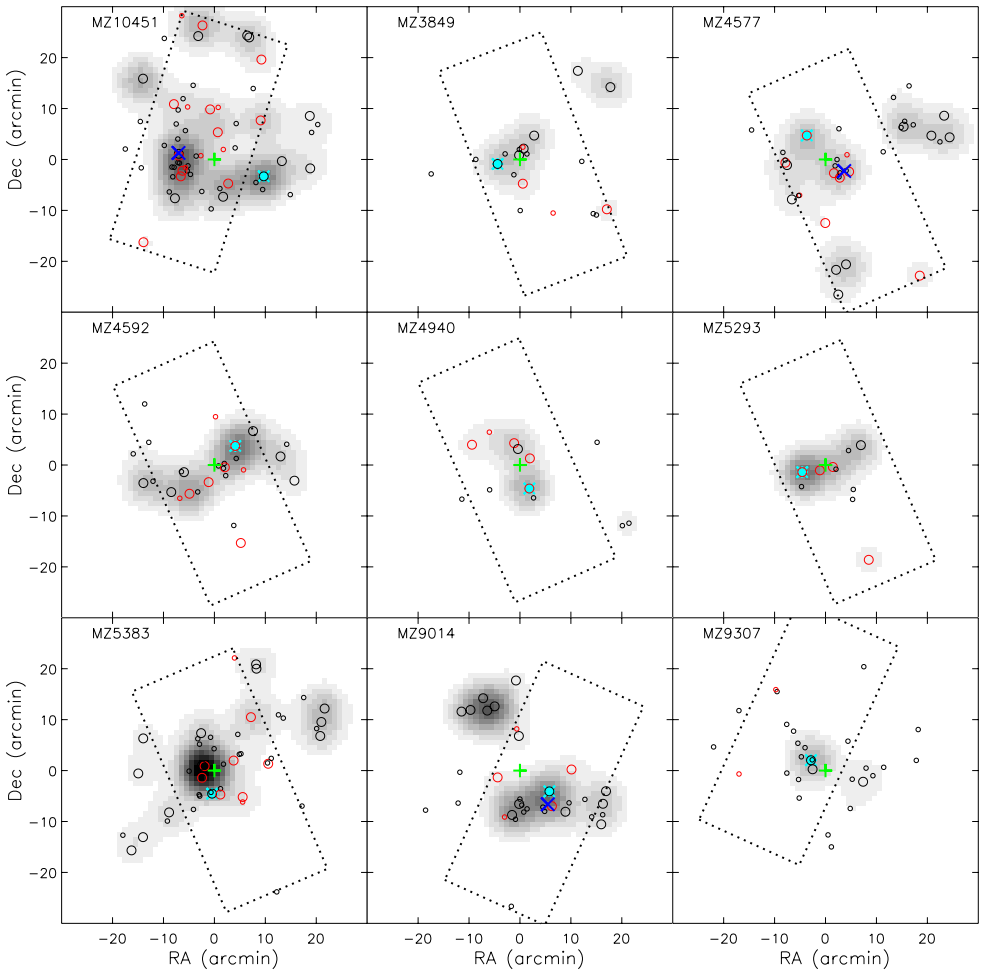

Figure 2. Spatial distribution of the group galaxies. Big circles represent group members with $M_R \leqslant -20$ and small ones $M_R > -20$. Red circles are the sources with 24 μm detection. Green plus signs indicate the luminosity-weighted group centers, and blue crosses denote the centroids of any detectable extended X-ray emission. The cyan stars are the BGGs within 1 Mpc of the group centers. Dotted rectangular regions show the MIPS 24 μm coverage in each field. Luminosity-weighted galaxy surface density maps are shown in gray scale, smoothed with a Gaussian kernel with FWHM $= 7'$ ($\sim$0.5 Mpc).

than $M_R = -19$ were excluded in the fraction calculations, due to incompleteness of our optical spectroscopy (and, likely, of our 24 μm data) at these magnitudes. Since only group members within the region of 24 μm coverage are considered for fraction calculations, most galaxies at large radii are also excluded. We note that the following results remain unchanged if we limit the fraction calculations to the galaxies covered by MIPS within 1 Mpc from the optical group centers.

4.1.1. Dependence of SF Fractions on Global Group Properties

In the top left panel of Figure 3, we plot the SF galaxy fractions in the nine groups as a function of group velocity dispersion. Most of the groups (six out of nine) show a high fraction (>50%) of SF galaxies. Two groups with $\sigma \sim 300$ km s^{-1}, MZ 3849 and MZ 9014, have smaller fractions of 43% and 33%, respectively. MZ 9307 is a peculiar case with zero fraction of SF galaxies: most of its members are dwarf galaxies with only two galaxies brighter than $M_R = -20$, and these are not SF, resulting in a SF fraction of zero with a large uncertainty. A Spearman correlation test shows that there is an anti-correlation between SF fractions and velocity dispersion (at a significance of 93%), but this trend is mostly driven by the two groups with smallest σ ($\sim$100 km s^{-1}) and highest SF fractions. The significance of the anti-correlation drops to 46% once these two groups are excluded.

If the velocity dispersion of a group correlates well with the mass of the group, which is true for a virialized system, then the lack of clear trend in SF fractions with velocity dispersion suggests that the SF properties of these groups do not depend strongly on total group mass. However, as evidenced by their irregular galaxy distribution and the general lack of a central BGG, the groups in our sample are not likely to be virialized, and their velocity dispersion might be a poor indicator of their masses. An alternative proxy for the group mass is the integrated stellar mass of group members. Yang et al. (2005) have demonstrated that the total stellar mass of group galaxies brighter than $M_R = -19.5 + 5 \log h$ correlates tightly with total group mass. To derive the total stellar mass of the groups, we used R-band magnitudes, calibrating the stellar mass calculation using a subset of our group galaxies that have SDSS five-band photometric data. For those galaxies, we can deduce their stellar masses using the spectral energy distribution (SED) fitting methods proposed by Blanton & Roweis (2007). The resulting stellar masses correlate well with the R-band magnitudes, with a 1σ scatter of 0.17 due to variations in stellar-mass-to-light ratio. We do not try to constrain the mass-to-light ratio using galaxy colors, because group galaxies outside our imaging region only have reliable R magnitudes. Furthermore, the uncertainty on stellar mass caused by such variations does not have a significant impact on the results in this paper.

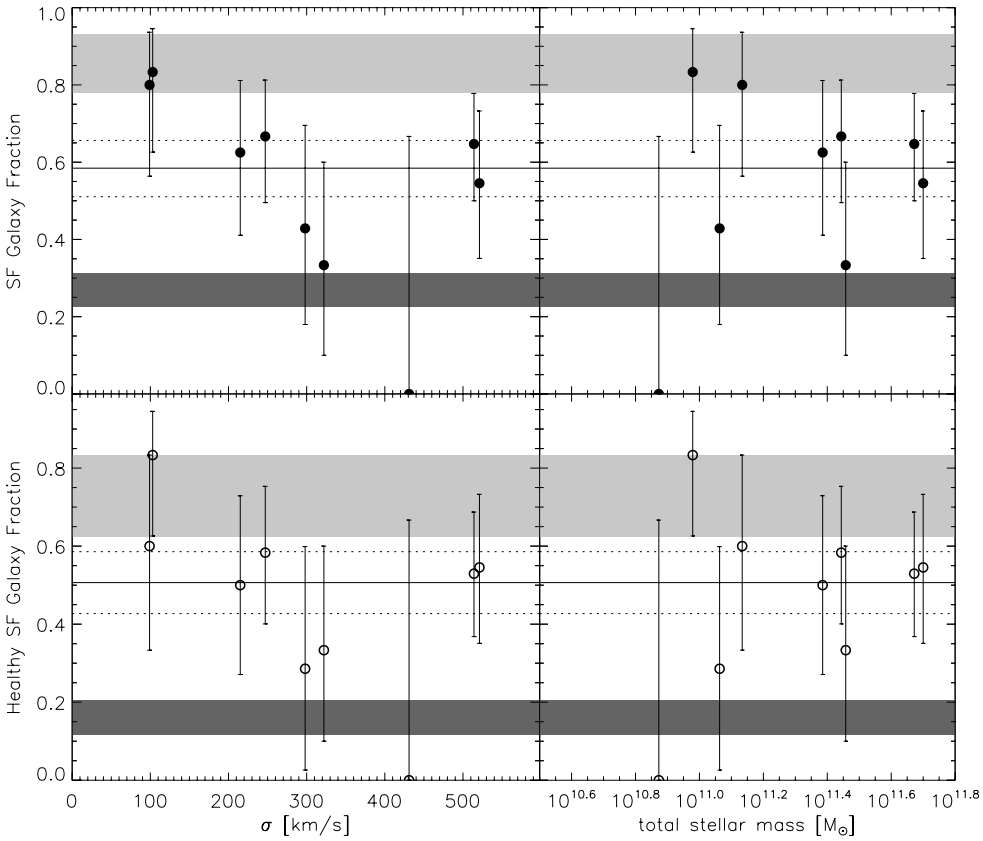

Figure 3. Top: SF galaxy fraction vs. (left) group velocity dispersion and (right) total stellar mass of the groups. The fraction is defined as the ratio of SF galaxies with SFR $> 0.1\ M_{\odot}\ \mathrm{yr}^{-1}$ to all galaxies with $M_R < -20$. Solid and dotted lines show the average fraction and its $\pm 1\sigma$ range. Gray shaded regions indicate the $\pm 1\sigma$ region of the average fractions of the field sample and dark shaded regions of the cluster sample. Bottom: same as the top panels but with the healthy SF galaxy fractions. The healthy SF fractions is defined as SF galaxies with specific SFR more than 20% of the typical specific SFR of the field galaxies from Salim et al. (2007).

Using the inferred correlation, we deduced the stellar mass for group galaxies in the full sample. From the top right panel of Figure 3, it is clear that there is no correlation between the SF fractions and the resulting total stellar mass of the groups. We also note that if we extend the SF fraction calculation to include galaxies 1 mag fainter ($M_R \leqslant -19$), the SF fractions in all groups become smaller, but they still show no trend with velocity dispersion nor with total stellar mass. As a comparison, we also calculate the SF galaxy fraction for the field and cluster samples. In the field, this fraction is $87^{+6}_{-9}\%$, about 30% higher than the mean SF fraction of all group galaxies ($58^{+7}_{-7}\%$). The two groups with the smallest velocity dispersions ($\sigma \sim 100\ \mathrm{km\ s}^{-1}$) have SF fractions consistent with the field average. The fraction in the cluster sample is $27^{+4}_{-4}\%$, about 30% lower than the group average.

We also note that the three groups with detectable extended X-ray emission do not show different SF fractions compared to those with no detection. Although the detection limits of our X-ray observations are not uniform due to variations in the useful exposure time, the fact that MZ 10451, the most X-ray luminous group with a luminosity typical of X-ray-selected high-σ groups, has an SF fraction of 65%, very similar to the average of our nine groups, argues against a significant correlation between SF fractions and the X-ray properties of our groups.

The weak dependence of SF fractions on group global properties is consistent with results from other studies of nearby groups (Balogh et al. 2004) and groups at intermediate redshifts (Wilman et al. 2005). This might be an indication that the SF properties of group galaxies are more affected by their immediate environment, e.g., local galaxy density, rather than the global environment. It could also suggest that the SF properties of the group members are not directly related to their present environment (Balogh et al. 2004).

4.1.2. Stacked SF Fractions

In nearby rich clusters, Bai et al. (2009) showed that the local SF fraction increases linearly from the cluster core to large radii (see also Mahajan & Raychaudhury 2009). For individual groups in our sample, there are too few galaxies to study this trend, so we stack all the groups together and plot the SF fraction against the projected distance from group luminosity-weighted centers in the middle panel of Figure 4. We note that not all annuli in this plot are uniformly covered by MIPS in all groups, but since only group members within the region of MIPS coverage are included in the fractions, partial coverage should not introduce systematic variations in the plot. In contrast to the rich clusters (shown in the left panel of Figure 4), SF fractions in groups show no clear dependence on the distance from the group centers and remain at a level higher than the outer region of the rich clusters ($>0.5R_{200}$, R_{200} is the radius within which the mean cluster density is 200 times the critical density of the universe at that redshift). Using a larger bin size does not change this result. We note that the left panel of Figure 4 is similar to Figure 7 of Bai et al. (2009), but with SFRs updated according to the prescription in Section 2.1.3. For our groups, some of which are likely not virialized, the virial radius is non-trivial to evaluate and may not be a meaningful measure, so we

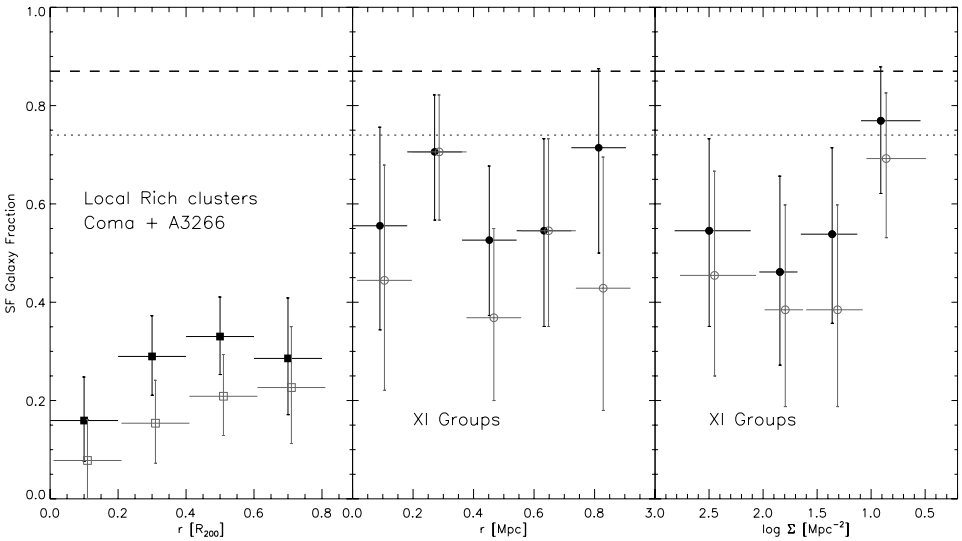

Figure 4. Left panel: SF galaxy fractions (filled black squares) and healthy SF galaxy fractions (gray open squares) in the nearby rich clusters Coma and A3266 as a function of projected distance (in units of R_{200}) from the cluster center. Middle panel: SF galaxy fractions (filled black circles) and healthy SF galaxy fractions (gray open circles) in groups as a function of projected distance from group centers. Right panel: SF fractions and healthy SF galaxy fractions in groups as a function of local projected galaxy density. In all three panels, the black dashed line is the average SF fractions in the field sample and the gray dotted line is the average healthy SF fractions in the field sample.

do not normalize the radii by R_{200} before stacking the group results.

The continuously decreasing SF fractions toward the cluster center could reflect a dependence of the SF properties on cluster properties that themselves depend on radius, such as local galaxy density or the density of the intracluster medium (ICM). If this is the case, the lack of a dependence of SF fractions on projected radius in groups could be a result of a breakdown of the correlation between galaxy density and projected distance rather than a breakdown of the correlation between SF fractions and galaxy density. The apparent displacements between the luminosity-weighted group centers and the galaxy density peaks seem to support this argument (see Figure 2). To check this possibility, we calculated the projected local galaxy density (Σ) for all the group galaxies using the distance to the second nearest neighbor (r_{2d}), $\Sigma = 3/(\pi r_{2d}^2)$. After assigning a local density to each group galaxy, we calculate the SF fractions in four density bins for all the galaxies brighter than $M_R = -20$ and within $10'$ (0.7 Mpc) away from the group centers. The spectroscopic survey is less complete in the outer regions ($>10'$) which could give rise to a systematically lower local density for galaxies at those radii. The density bins are selected to have roughly the same number of galaxies in each bin, and the highest density bin has density comparable to the value at $0.2R_{200}$ of the clusters. In the right panel of Figure 4, we plot the SF fractions as a function of density. However, the SF fractions of all three high-density bins remain approximately constant at a level higher than the fractions in the cluster. The lowest-density bin has a marginally significant higher SF fraction, and it is consistent with the average field value. This could be evidence of an anti-correlation between density and SF fractions, but the large uncertainties preclude robust conclusions in this regard (51% probability from a Spearman test).

4.2. Specific SFR of Group Galaxies and Healthy SF Galaxy Fractions

In the previous section, we focused on the study of the total current SFR in a galaxy. However, a fixed SFR can contribute substantially to the total stellar mass, color, and optical spectrum of a small galaxy but little to a massive one. In this sense, the specific SFR, i.e., the total SFR normalized by the stellar mass of a galaxy, is a better measure of the relative importance of SF in different galaxies. Because the stellar mass of a galaxy is the integral of the past SFR, the specific SFR, to first order, is also a measure of star formation history. Many studies (Gavazzi & Scodeggio 1996; Boselli et al. 2001; Kauffmann et al. 2004) have indicated that the specific SFR depends primarily on galaxy mass, with any environmental dependence being of secondary importance. To disentangle the environmental dependence from the mass dependence, we derived the specific SFRs of our group galaxies and compared them to those of cluster and field galaxies.

In Figure 5, we plot the specific SFRs of group galaxies as a function of their stellar mass. The SF group galaxies with $M_* < 10^{10.5}\,M_\odot$ concentrate, although with a fair amount of scatter, on a SF sequence (e.g., Salim et al. 2007). The more massive galaxies generally show lower specific SFRs. Along with group galaxies, we plot the SF sequence of a large sample of local SF galaxies from Salim et al. (2007). Using UV data from *Galaxy Evolution Explorer* (*GALEX*) along with SDSS data, Salim et al. (2007) measured the SFRs of ~50,000 nearby galaxies and calculated the mode, i.e., the value that occurs most often, of the specific SFR as a function of stellar mass. They characterized this function with a Schechter function, plotted as a dash-dotted curve in Figure 5. It shows for each stellar mass the most frequently observed specific SFRs of field galaxies. Although Salim et al. (2007) used a different SFR indicator, their UV-inferred and IR-inferred SFRs show good overall agreement, with a systematic offset of just ~0.02 dex and scatter of ~0.5 dex (Salim et al. 2009). The difference between their IR SFR estimation and ours introduces a systematic difference ~0.1 dex in the SFR range of our interest (Salim et al. 2009). To compare with their SF sequence, we also calculate the mode of the specific SFRs for the group galaxies, as well as the modes for our field and cluster samples, in four stellar mass bins. To be consistent, we only calculate the mode for SF galaxies with SFR $> 0.1\,M_\odot\,\mathrm{yr}^{-1}$, which is the detection limit of the group

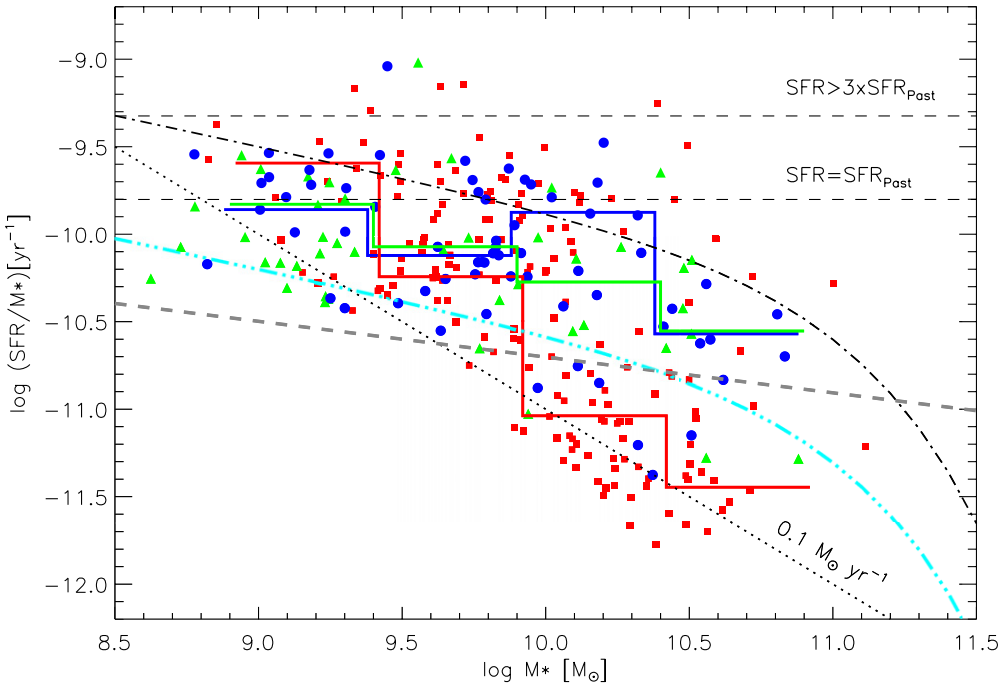

Figure 5. Specific SFRs (SFR/M_*) of galaxies as a function of stellar mass. Filled blue circles, green triangles, and red squares represent group, field, and cluster galaxies, respectively. Black dash-dotted curve indicates the most frequent specific SFRs of field galaxies as determined by Salim et al. (2007), and the cyan triple-dot-dashed line represents 20% of this value, used to define "healthy" SF galaxies. Blue, green, and red histograms show the modes of the specific SFRs for SF galaxies with SFR $> 0.1\,M_\odot\,\mathrm{yr}^{-1}$ in our group, field, and cluster sample, respectively. The black dotted line shows the $0.1\,M_\odot\,\mathrm{yr}^{-1}$ detection limit of our 24 μm group data. The gray dashed line is the SF dividing line for passive/active galaxies in Weinmann et al. (2006). The two black dashed horizontal lines correspond to birthrates of 3 and 1.

galaxies. This detection limit is higher than that of the UV data used by Salim et al. (2007), which are sensitive down to at least SFR $\sim 0.01\,M_\odot\,\mathrm{yr}^{-1}$. Therefore, the modes of the specific SFRs of the galaxies calculated here only represent the typical value of the upper envelope in the distribution of specific SFR versus stellar mass, and they could overestimate the actual typical specific SFRs.

The modes of our field sample, although subject to large uncertainties due to the small sample size, generally follow the SF sequence found by Salim et al. (2007), but are systematically lower by 0.3 dex. Part of this difference comes from the systematic difference in SFR estimates (∼0.1 dex). This systematic difference is not significant though, given the intrinsic scatter in specific SFR along the SF sequence (0.5 dex; Salim et al. 2007) and the scatter in the correlation between the UV- and IR-inferred SFRs. At $M_* < 10^{10}\,M_\odot$, the SF galaxies in clusters, groups, and the field occupy similar regions in the plot and do not show any significant difference in their distribution. However, in this mass range, the 24 μm sensitivity limits us from detecting SF galaxies with relatively low specific SFRs. The similarity therefore only shows that the upper envelope of the specific SFR versus stellar mass distribution is broadly similar in all environments within this mass range. However, it is not clear whether there is a different distribution for SF galaxies below our detection limit. At $M_* > 10^{10}\,M_\odot$, the typical specific SFRs of the XI group galaxies are still very similar to those of the field. However, the cluster SF galaxies show much lower typical specific SFRs compared to group and field galaxies of similar mass. This difference is mostly due to a fraction (14%) of massive galaxies with very low specific SFR $< 10^{-11}\,\mathrm{yr}^{-1}$ that is the most prominent in clusters. The SFRs of these galaxies are very close to our detection limit, and their 24 μm luminosities are only a few times higher than what is expected from the cold dust emission of an old stellar population. The SF properties of these massive galaxies are very similar to "dusty red galaxies" found in the A901/2 super cluster (Wolf et al. 2009; Gallazzi et al. 2009). In order to find out if the massive SF galaxies are the same population as the dusty red galaxies, we compare their colors and morphologies with the galaxies in the Coma cluster where we have this information. We confirm that the majority of the massive SF galaxies are indeed red in color. However, the morphologies of these galaxies are typically S0/Es, differing from the dust red galaxies discussed by Wolf et al. (2009), which are mostly passive spiral galaxies (Sa/Sb).

In the top panel of Figure 6, we show the fractions of galaxies with SFR $> 0.1\,M_\odot\,\mathrm{yr}^{-1}$ in four stellar mass bins. For both groups and the field, the fractions of galaxies with SFR $> 0.1\,M_\odot\,\mathrm{yr}^{-1}$ are all >50% at $M_* > 10^{9.5}\,M_\odot$. This high detection fraction helps to support the robustness of the typical specific SFRs derived for these two samples in this mass range. In the lowest mass bin, the detection fractions in all environments are quite low, and we begin to lose SF galaxies on the SF sequence due to the detection limit. In this mass bin, the derived specific SFR modes only represent the typical value of a subset of the SF galaxies. In all mass bins, the SF fractions in groups are lower than those in the field, with the clusters showing the lowest fractions. For galaxies with $M_* > 10^{10.5}\,M_\odot$, the SF fraction in clusters is comparable to that in the groups. However, it is clear from Figure 5 that the typical specific SFR of cluster galaxies in this mass range is lower than the value of the group and field galaxies; defining SF galaxies using a fixed SFR limit for galaxies of differing mass clearly fails to distinguish these different populations of SF galaxies. To take this mass dependence of the specific SFRs into account, we assume that the typical specific SFR of field galaxies is the value for a galaxy unaffected by its environment, and define "healthy" SF galaxies

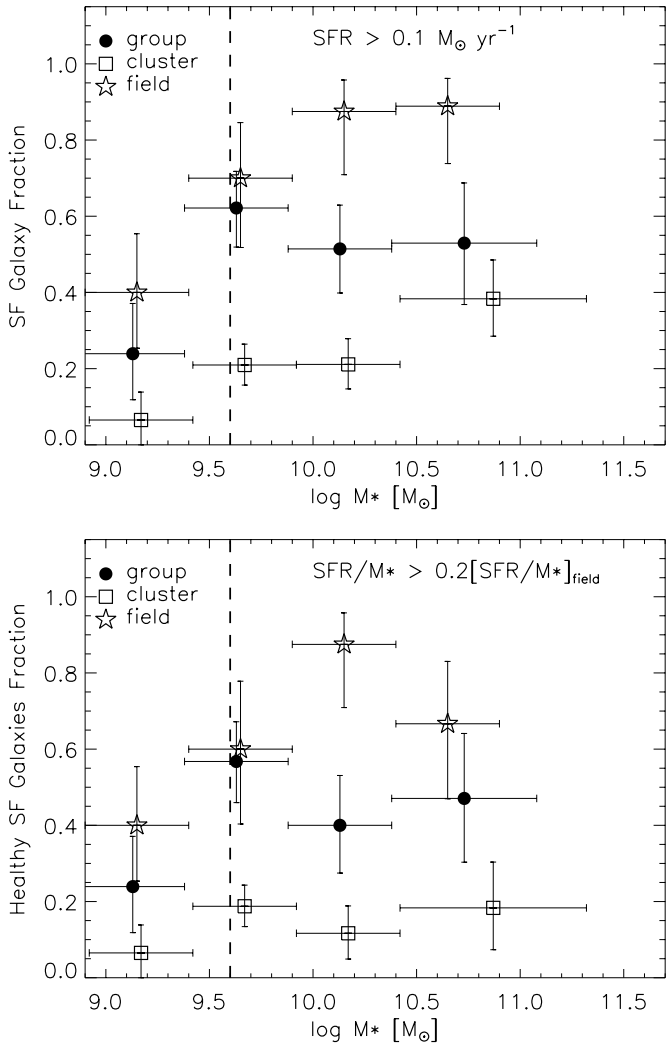

Figure 6. Top panel: SF galaxy fraction as a function of stellar mass. Filled circles, open stars, and open squares show the group, field, and cluster galaxies, respectively. Bottom panel: as above, but for the healthy SF galaxy fractions. Dashed vertical lines are shown at $M_* = 10^{9.6}\,M_\odot$, corresponding to $M_R = -20$.

as galaxies with specific SFR at least 20% of the typical value of field SF galaxies of the same mass, as found by Salim et al. (2007). If we take into consideration the systematic difference between the SF sequences obtained from our field sample and from the SDSS SF galaxy sample with UV data, and assume that the average scatter in the SF sequence is the same as that of the SDSS SF galaxies of Salim et al. (2007), then 75% of the SF galaxies in our field sample should have specific SFRs above this limit. In the bottom panel of Figure 6, we show the healthy SF galaxy fractions as a function of stellar mass. In the three high-mass bins, where we are sensitive to all the healthy SF galaxies, the fractions in our field sample are all above 60% and generally consistent with the 75% from the above expectation. The fractions in groups range from 40% to 60%, all lower than in the field. But the difference is most pronounced in the $M_* = 10^{9.9}$–$10^{10.4}\,M_\odot$ bin and is not significant in the other mass bins. In clusters, the fractions remain very low in all mass bins, 10%–20%. Although the SF fraction in clusters is about 40% at $M_* > 10^{10.5}\,M_\odot$, almost as high as that in groups, the healthy SF fraction is only 20%, much lower than that in groups.

It is clear from Figures 5 and 6 that using a fixed SFR cut to define SF galaxies and assess the SF properties in different environments may not be able to differentiate massive galaxies with lower than typical SFR from low-mass normal SF galaxies. Therefore, we repeat the analysis of Section 4.1 by calculating the healthy SF galaxy fraction for each group. We limit the calculation to galaxies with $M_* > 10^{9.6}\,M_\odot$, which corresponds to the $M_R = -20$ mag cut used for calculating the SF fractions. Above this limit, our data are sensitive to all the healthy SF galaxies. In the bottom panels of Figure 3, we plot the healthy SF galaxy fractions against group velocity dispersion and total stellar mass. Again, there is no obvious systematic trend between healthy SF fraction and velocity dispersion or total stellar mass. The probability of an anti-correlation between healthy SF fractions and velocity dispersion is only 84%. The average fraction in groups is 51^{+8}_{-8}%, lower than that of the field (74^{+9}_{-11}%) but higher than in clusters (16^{+4}_{-4}%).

The lack of dependence of healthy SF fractions on group velocity dispersion and total stellar mass would appear to be in contrast with the study of Weinmann et al. (2006). Using a galaxy group catalog constructed from SDSS data, Weinmann et al. (2006) divide galaxies into early-type and late-type galaxies, based on criteria very similar to what we use to define healthy SF galaxies, but they found that the fraction of early-type galaxies in groups increases with group halo mass. Specifically, they define early-type galaxies as both red in color and "passive" in terms of their SF properties. Because only 1% of their group population is blue and "passive," the early-type galaxies are approximately equivalent to passive galaxies. They adopt a mass-dependent specific SFR cut to divide passive and active galaxies, which is very similar to our criteria for healthy SF galaxies (shown as the gray dashed line in Figure 5). To directly compare with their results, we use the same SFR criteria to define passive galaxies in our group sample and calculate the passive galaxy fractions for galaxies with $M_* > 10^{10}\,M_\odot$, equivalent to the magnitude cut of Weinmann et al. (2006). In Figure 7, we show this fraction as a function of group velocity dispersion. Again, similar to what we find in terms of healthy SF fractions, the fractions of passive galaxies in our group sample do not show any strong trend with velocity dispersion. A Spearman test shows that the probability of correlation is only 25%. This apparent discrepancy could be due to small number statistics owing to the limited size of our group sample. In fact, within the rather large statistical uncertainties, the majority of our nine groups do show fractions consistent with the mean trends found by Weinmann et al. (2006). In addition, the discrepancy could arise partly from differences in the adopted group definitions. Weinmann et al. (2006) select groups using a halo-based group finder (Yang et al. 2005) while the MZ sample is based on a friends-of-friends algorithm. The halo-based group finder assumes that groups are virialized systems, but this assumption is unlikely to hold in general for the groups in our sample, where some systems are probably still in the process of collapsing and so are not yet fully virialized.

Finally, we also examined the healthy SF fractions as a function of radius from the group centers and the local projected galaxy density. These fractions are shown as gray squares in Figure 4. Although the healthy SF fractions in all environments are lower than the "standard" SF fractions, the general results obtained earlier remain unchanged: there is no systematic dependence of healthy SF fractions on the distance from the group centers. although there might be a weak anti-correlation between healthy SF fractions and projected galaxy density. The

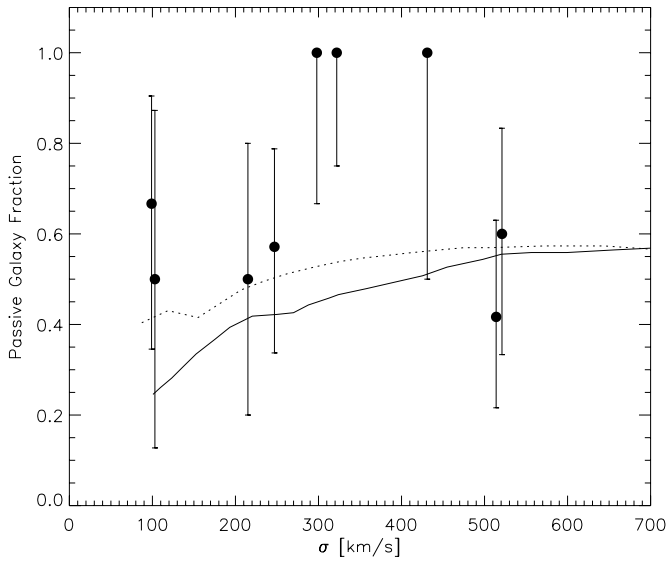

Figure 7. Passive galaxy fractions as a function of group velocity dispersion. The passive galaxies are defined by the criteria in Weinmann et al. (2006) and the curves are the trends found by these authors using an SDSS group catalog. The dotted curve is derived by estimating SDSS group masses from velocity dispersion, and the solid line from total luminosity (Weinmann et al. 2006).

healthy SF fractions of groups are higher in all density bins than the fractions seen in the outskirts of clusters.

4.3. SF History of Group Galaxies

As mentioned, the current specific SFR of a galaxy provides a rough measure of its star formation history. The specific SFR can be directly related to the birthrate, which is defined as the current SFR normalized by its past average. Given a gas recycling fraction R and stellar age τ, the birthrate $b = \frac{\mathrm{SFR}}{\langle \mathrm{SFR}_{\mathrm{past}} \rangle} = \frac{\mathrm{SFR}\cdot\tau}{M_*}(1-R)$ (Kennicutt et al. 1994). Assuming $R = 0.5$ and the age of the universe at $z = 0.06$ as an upper limit to τ (Brinchmann et al. 2004), we can calculate the upper limit of the birthrate for group galaxies. As shown in Figure 5, most of the SF group galaxies with $M_* < 10^{10.4}\,M_\odot$ have $b \approx 1$, indicating they are forming stars more or less at the same rate as the past average. If we define galaxies with current SFRs 3 times larger than the past average as starburst galaxies (Brinchmann et al. 2004), only one group galaxy fulfills this criterion. For more massive group galaxies, their current SFRs are generally lower than their past average, consistent with the trend for field galaxies. In clusters, there is a relatively large number of SF galaxies with current SFR significantly lower than their past average.

5. DISCUSSION

5.1. The SF Fraction in Different Environments

On average, the SF fraction in our group sample is 30% lower than that in the field. Even though this deficit of SF galaxies may be minimal in the least massive systems and the lowest-density regions, it prevails in the typical environment of our group population. This result is consistent with the higher fraction of passive galaxies found in many different group samples at different redshift ranges compared to the field (Balogh et al. 2004, 2009; Wilman et al. 2005; Jeltema et al. 2007). On the other hand, when compared to the clusters A3266 and Coma, the SF fraction in groups is generally 30% higher. The decreasing SF fractions in more massive structures could suggest an environmental effect, but it does not directly imply an environmental suppression of the galaxy SF. Many studies have shown that massive galaxies formed their stars early on in a short time period while less massive galaxies evolved more gradually (e.g., Cowie et al. 1996; Heavens et al. 2004). This suggests that the stellar mass is probably the most important variable that regulates the star formation history of a galaxy (e.g., Noeske et al. 2007). If galaxy clusters and groups, which originated from the highest density perturbations in a cold dark matter (CDM) universe, also preferentially host more massive galaxies (Bardeen et al. 1986), then the observed difference in the SF properties between high- and low-density environments was seeded at the beginning of the universe. This is considered to be the "nature" scenario of galaxy evolution. However, the fact that the healthy SF galaxy fractions, which by definition already take into account the stellar mass dependence of the SF properties, also show an increasing deficit in denser environments which persists across a large stellar mass range, suggests this scenario cannot fully explain those differences and that some additional "nurture" process that invokes environmental effects is needed (Christlein & Zabludoff 2005; Baldry et al. 2006).

5.2. Comparing Groups with the Field

Even though the group galaxies have, on average, a much lower SF fraction than the field, the typical specific SFRs of group SF galaxies are not very different from those of field galaxies at $M_* > 10^{9.6}\,M_\odot$. Similar to our result, Vulcani et al. (2010) and K. D. Tyler et al. (2010, in preparation) also found the specific SFRs of group and field galaxies of higher redshift ($z > 0.3$) are not very different. Therefore, if the much lower SF fractions in groups is caused by some environmental mechanism, the transformation needs to happen on a short timescale. Such a mechanism should quickly turn normal SF galaxies into quiescent ones without affecting the overall typical specific SFRs too much. Galaxy–galaxy interactions appear to be a likely candidate for this mechanism. These interactions can trigger starbursts in galaxies and cause them to exhaust their gas fuel quickly (Mihos & Hernquist 1994). This mechanism is expected to be most efficient in poor groups. The tentative dependence of SF fractions on the local galaxy density also favors galaxy–galaxy interactions as the dominant mechanism.

Miles et al. (2004) found a prominent dip at $M_R \approx -19.5$ in the optical luminosity functions of poor groups and attributed it to galaxy merging by dynamical friction, which preferentially depletes the intermediate-luminosity galaxies. Corresponding to the dip, there is also a bump at brighter magnitudes ($M_R \approx -20.5$), which can be explained by the boosted galaxy number resulting from merged lower-mass galaxies. Interestingly, the healthy SF fraction in our group sample also shows a potential dip at $M_* \approx 10^{10.1}\,M_\odot$. In this stellar mass bin, the group sample shows the largest deviation from the field sample, with ~40% fewer healthy SF galaxies. In the two neighboring mass bins, the fractions in the group sample are still lower than that in the field, but the differences are not significant. Incidentally, the dip of the healthy SF fraction occurs roughly in the stellar mass range where the bump of the optical luminosity function is located ($M_* \approx 10^{9.8}\,M_\odot$). This supports a scenario in which there are relatively more merged galaxies in this stellar mass range which have exhausted their gas fuel at the early starburst stage of the interaction and now show little SF. However, a larger sample of group and field galaxies would be needed to confirm this possible dip in healthy SF fractions.

If such interaction-triggered starbursts are responsible for eventual SF suppression, the detection of galaxies with enhanced star formation could be direct evidence of such processes in action. However, we only detect one such galaxy in our sample. Similar to our work, Balogh et al. (2009) also failed to detect galaxies with enhanced star formation in their intermediate redshift group sample. However, the detectability of such a population in groups depends sensitively on the duration of the interaction-induced starburst. Using hydrodynamical simulations, Cox et al. (2006, 2008) investigated properties of merger-driven starbursts and the effects of employing different supernova feedback models. Although their simulations suggest that the amount of the total gas consumption of the merger-induced star formation that is directly related to SF suppression is invariant with respect to the choice of feedback model, the duration of the starbursts does vary from model to model. Their "stiff" feedback model assumes the SF gas has an equation of state $P \sim \rho^2$ while their "soft" model assumes the gas is isothermal. The stiff feedback model predicts a starburst timescale of $\geqslant$0.5 Gyr, whereas the soft model results in a much short timescale $\geqslant$0.1 Gyr. If we adopt the timescale given by the stiff feedback model, the starburst fraction of $<$1% found for the present group sample sets an upper limit of 10% for the fraction of galaxies that have experienced such a merger-induced starburst within the last 5 Gyr. This fraction falls short of explaining the 30% deficit of SF galaxy found in current groups population compared to the field. However, if we adopt the shorter timescale given by the soft feedback model, enough merger-induced starbursts will have occurred within the last 2–4 Gyr to explain the deficit.

In addition to galaxy–galaxy interactions, other mechanisms could also be at work within the group environment. Even though the gas density of the intragroup medium is usually not sufficient to ram pressure strip the cold disk gas in a galaxy, it could efficiently strip any hot gaseous halo (Rasmussen et al. 2006a; Kawata & Mulchaey 2008; McCarthy et al. 2008). This would cut off the supply that replenishes cold gas and eventually shut down the star formation in galaxies. The timescale of this quenching process, the so-called strangulation, is much longer ($>$1 Gyr). If it is the dominant process responsible for the deficit of SF galaxies, we would expect to see many SF galaxies with suppressed SFRs. This is inconsistent with the similar typical specific SFR we found in our group and field samples across a large stellar mass range, suggesting that strangulation is probably not the dominant mechanism for galaxies with $M_* > 10^{9.6}\,M_\odot$ in the poor groups studied here. In X-ray luminous groups, however, this mechanism may become more important.

5.3. Comparing Groups with Clusters

In hierarchical structure formation, galaxy clusters are assembled from lower mass halos and the galaxies in clusters might have been residing in group environments before they finally fell into clusters. This makes "preprocessing" in groups potentially important for cluster galaxies (Zabludoff & Mulchaey 1998). However, the importance of preprocessing depends on the accretion history of clusters. Using CDM *N*-body simulations, Berrier et al. (2009) claimed that the majority of cluster galaxies (70%) have never resided in a group environment before they fell into the cluster, and therefore that preprocessing in group environments could not play a significant role in explaining the difference between cluster and field galaxies. This result seems to be at odds with the observation that about half of the galaxy population resides in group environments in the nearby universe (Eke et al. 2004, 2005; McGee et al. 2009), because it would mean that clusters preferentially accrete isolated galaxies rather than galaxies in groups. The apparent discrepancy, again, is likely related to differences in the adopted group definition. Berrier et al. (2009) define group members as the halos within the virial overdensity boundary of the hosting dark matter halos. This definition results in a much smaller fraction ($\sim$15%) of galaxies residing in group environments compared to those found by the friends-of-friends algorithms typically used to identify groups in observational samples. Given the small fraction of galaxies residing in groups according to the former definition, it is no surprise that the majority of the galaxies falling into clusters have never been preprocessed within a group environment by this definition. On the other hand, if we follow the much more relaxed group definition as adopted in friends-of-friends algorithms, we would expect a much higher fraction of cluster galaxies to have been part of the group environment prior to falling into clusters. However, even if all the cluster galaxies have been in groups, the lower fraction of SF galaxies in clusters in a large stellar mass range compared to the fraction found in the XI groups suggests that preprocessing in groups is not sufficient to explain the deficiency of SF galaxies in clusters. This is reinforced by the fact that even in the highest density regions of our groups, the SF fraction is still higher than the fraction found in the outskirts of clusters. To explain the low SF fractions in clusters, either an environmental mechanism that works in group environments must continue to work in clusters, or some other cluster-specific environmental mechanism must be invoked. In either case, further processing of SF galaxies within the cluster environment is required.

Not only are the SF fractions of cluster galaxies on average smaller than in groups, but the SF galaxies in clusters have smaller specific SFRs at $M_* > 10^{10}\,M_\odot$ (see also Vulcani et al. 2010). Such differences strongly support further SF suppression in clusters. Bai et al. (2006, 2009) found that the IR luminosity function of nearby rich clusters has the same shape at the bright end ($L_{\rm IR} > 10^{43}$ erg s^{-1}) as that of field galaxies. The galaxies that contribute to the bright end of the IR luminosity function are galaxies with SFR $> 0.3\,M_\odot$ yr^{-1}, which constitute the upper envelope of the specific SFR versus stellar mass distribution of cluster galaxies (cf. Figure 5). The similarity of the bright-end shape of the IR luminosity function in different environments is corroborated by the similar upper envelope of the specific SFR versus stellar mass distribution found here. Bai et al. (2009) suggest this similarity points to a fast acting SF suppression mechanism in clusters, for example, ram pressure stripping, that produces few galaxies in transition. However, the comparison of the specific SFRs of cluster SF galaxies to those in the groups and field does reveal a population of massive SF galaxies ($M_* > 10^{10}\,M_\odot$), with suppressed but not totally extinguished SF, predominantly seen in clusters. This difference does not necessarily exclude ram pressuring stripping as an important mechanism in clusters, however, because massive galaxies are less vulnerable to such processes and could still retain some of their gas following a stripping event. The residual gas in those massive galaxies could sustain low-level SF for a much longer time.

6. SUMMARY

We have presented the first mid-IR study of nearby groups with complete optical spectroscopy and X-ray data. The nine groups in our sample span a wide range in velocity disper-

sion (100–500 km s^{-1}), X-ray properties, richness, and galaxy distribution. These groups are typical of the galaxy groups that make up more than half of the galaxy population in the nearby universe, and they are likely covering a wide range of evolutionary states. We analyzed the SF properties of the group galaxies from their MIPS 24 μm emission and tested for correlations with global group properties. We also compared the SF properties of the group galaxies with those of cluster and field galaxies at the same redshifts to investigate the environmental effect on galaxy evolution. Our major results are summarized as follows.

1. The projected galaxy distributions of the nine groups show large variations, from more concentrated and circular distributions in the most massive groups ($\sigma \sim 500$ km s^{-1}) to filamentary structures in the least massive ones ($\sigma \sim 100$ km s^{-1}). This variation, along with the lack of a dominant BGG in the group center and the generally low level of extended X-ray emission, suggests that some of these systems are not yet virialized but still in the process of collapsing.
2. On average, the SF galaxy fraction (SFR $> 0.1\,M_\odot$ yr^{-1}, $M_R < -20$) in our group sample is about 30% lower than in a comparison field sample extracted from the same data, and 30% higher than in our comparison cluster sample. The SF fraction of our groups does not show a strong systematic dependence on group global properties such as velocity dispersion, total stellar mass, or the presence of detectable diffuse X-ray emission. However, the two groups with the smallest velocity dispersion ($\sigma \approx 100$ km s^{-1}) do show the highest SF fractions, at a level comparable to that of the field. These conclusions remain unchanged if only considering the "healthy" SF galaxy fractions (SFR/$M_* > 0.2$[SFR/M_*]$_{\rm field}$, $M_* > 10^{9.6}\,M_\odot$).
3. There is no strong dependence of the SF fraction on the radial distance from the group center. The 24 μm SF fraction in the groups is, at all radii, larger than the corresponding fraction in the outskirts ($\sim R_{\rm vir}$) of rich clusters at similar redshifts. There is a weak trend of SF fractions decreasing with increasing projected galaxy density, with the lowest-density regions having an SF fraction comparable to the field population. Even in the highest density regions of groups, the SF fraction is still larger than the SF fraction in the outer regions of clusters. In addition, the healthy SF fractions of cluster galaxies across a large stellar mass range are all at least 20% lower than those in groups. These pieces of evidence strongly suggest that preprocessing of galaxies in group environments prior to infall into clusters is not a sufficient explanation for the lower fraction of SF galaxies in clusters and that further processing by the cluster environment is required.
4. The typical specific SFRs of SF galaxies in groups are very similar to that in the field across a wide mass range ($M_* > 10^{9.6}\,M_\odot$), favoring a quickly acting mechanism that suppresses star formation to explain the overall smaller fraction of SF galaxies in groups. The healthy SF fractions in groups show a possible dip at $M_* \approx 10^{10.1}\,M_\odot$, corresponding to the bump seen in the optical luminosity function of poor groups (Miles et al. 2004). This is consistent with the speculation that galaxy merging by dynamical friction preferentially depletes intermediate-luminosity galaxies, which become subject to rapid gas consumption during the interaction, resulting in a population of galaxies of high stellar mass and a relatively low fraction of healthy SF galaxies. If galaxy–galaxy interactions are responsible for the deficit of SF galaxies in groups, then our non-detection of a significant starburst population among current group members does indeed imply a short timescale for any merger-induced starburst stage ($\sim$0.1 Gyr). This agrees well with a supernova feedback model that assumes an isothermal state for the SF gas.
5. At $M_* > 10^{10}\,M_\odot$, the SF galaxies in clusters show much lower typical specific SFRs than galaxies in groups and the field, due to a more significant population of massive galaxies with very low SFR (14% of all the cluster galaxies with $M_* > 10^{10}\,M_\odot$). This could result from ram pressure stripping being less efficient in removing gas from more massive cluster galaxies, allowing such galaxies to sustain low-level star formation fueled by a residual gas reservoir.

We thank Augustus Oemler, Alan Dressler, and Ann Zabludoff for useful discussions, and the referee for insightful comments and suggestions. J.R. acknowledges support provided by the National Aeronautics and Space Administration through Chandra Postdoctoral Fellowship Award Number PF7-80050 issued by the Chandra X-ray Observatory Center, which is operated by the Smithsonian Astrophysical Observatory for and on behalf of the National Aeronautics and Space Administration under contract NAS8-03060. We also acknowledge partial support for this work from NASA-JPL grant 1310258, NASA grant NNG04GC846, and NSF grant AST-0707417. This publication makes use of data products from the Two Micron All Sky Survey, which is a joint project of the University of Massachusetts and the Infrared Processing and Analysis Center/California Institute of Technology, funded by the National Aeronautics and Space Administration and the National Science Foundation. This research has made use of the NASA/IPAC Extragalactic Database (NED), which is operated by the Jet Propulsion Laboratory. California Institute of Technology, under contract with the National Aeronautics and Space Administration.

REFERENCES

Bai, L., Rieke, G. H., Rieke, M. J., Christlein, D., & Zabludoff, A. I. 2009, ApJ, 693, 1840
Bai, L., Rieke, G. H., Rieke, M. J., Hinz, J. L., Kelly, D. M., & Blaylock, M. 2006, ApJ, 639, 827
Bai, L., et al. 2007, ApJ, 664, 181
Baldry, I. K., Balogh, M. L., Bower, R. G., Glazebrook, K., Nichol, R. C., Bamford, S. P., & Budavari, T. 2006, MNRAS, 373, 469
Baldry, I. K., Glazebrook, K., Brinkmann, J., Ivezić, Ž., Lupton, R. H., Nichol, R. C., & Szalay, A. S. 2004, ApJ, 600, 681
Balogh, M., et al. 2004, MNRAS, 348, 1355
Balogh, M. L., et al. 2009, MNRAS, 398, 754
Bardeen, J. M., Bond, J. R., Kaiser, N., & Szalay, A. S. 1986, ApJ, 304, 15
Beers, T. C., Flynn, K., & Gebhardt, K. 1990, AJ, 100, 32
Berrier, J. C., Stewart, K. R., Bullock, J. S., Purcell, C. W., Barton, E. J., & Wechsler, R. H. 2009, ApJ, 690, 1292
Bertin, E., & Arnouts, S. 1996, A&AS, 117, 393
Bigelow, B. C., & Dressler, A. M. 2003, Proc. SPIE, 4841, 1727
Blanton, M. R., & Roweis, S. 2007, AJ, 133, 734
Boselli, A., Gavazzi, G., Donas, J., & Scodeggio, M. 2001, AJ, 121, 753
Brand, K., et al. 2009, ApJ, 693, 340
Brinchmann, J., Charlot, S., White, S. D. M., Tremonti, C., Kauffmann, G., Heckman, T., & Brinkmann, J. 2004, MNRAS, 351, 1151
Buat, V., et al. 2007, ApJS, 173, 404
Christlein, D., & Zabludoff, A. I. 2005, ApJ, 621, 201
Colless, M., et al. 2001, MNRAS, 328, 1039
Cowie, L. L., Songaila, A., Hu, E. M., & Cohen, J. G. 1996, AJ, 112, 839
Cox, T. J., Jonsson, P., Primack, J. R., & Somerville, R. S. 2006, MNRAS, 373, 1013
Cox, T. J., Jonsson, P., Somerville, R. S., Primack, J. R., & Dekel, A. 2008, MNRAS, 384, 386

Dressler, A., Rigby, J., Oemler, A., Fritz, J., Poggianti, B. M., Rieke, G., & Bai, L. 2009, ApJ, 693, 140
Eke, V. R., Baugh, C. M., Cole, S., Frenk, C. S., King, H. M., & Peacock, J. A. 2005, MNRAS, 362, 1233
Eke, V. R., et al. 2004, MNRAS, 348, 866
Fadda, D., Biviano, A., Marleau, F. R., Storrie-Lombardi, L. J., & Durret, F. 2008, ApJ, 672, L9
Gallazzi, A., et al. 2009, ApJ, 690, 1883
Gavazzi, G., & Scodeggio, M. 1996, A&A, 312, L29
Geach, J. E., et al. 2006, ApJ, 649, 661
Geller, M. J., & Huchra, J. P. 1983, ApJS, 52, 61
Gómez, P. L., et al. 2003, ApJ, 584, 210
Gordon, K. D., et al. 2005, PASP, 117, 503
Haines, C. P., Smith, G. P., Egami, E., Okabe, N., Takada, M., Ellis, R. S., Moran, S. M., & Umetsu, K. 2009a, MNRAS, 396, 1297
Haines, C. P., et al. 2009b, ApJ, 704, 126
Hambly, N. C., et al. 2001, MNRAS, 326, 1279
Heavens, A., Panter, B., Jimenez, R., & Dunlop, J. 2004, Nature, 428, 625
Helsdon, S. F., & Ponman, T. J. 2000, MNRAS, 315, 356
Hou, A., Parker, L. C., Harris, W. E., & Wilman, D. J. 2009, ApJ, 702, 1199
Iovino, A., et al. 2010, A&A, 509, A40
Jeltema, T. E., Mulchaey, J. S., Lubin, L. M., & Fassnacht, C. D. 2007, ApJ, 658, 865
Jones, D. H., et al. 2009, MNRAS, 399, 683
Kauffmann, G., White, S. D. M., Heckman, T. M., Ménard, B., Brinchmann, J., Charlot, S., Tremonti, C., & Brinkmann, J. 2004, MNRAS, 353, 713
Kauffmann, G., et al. 2003, MNRAS, 341, 54
Kawata, D., & Mulchaey, J. S. 2008, ApJ, 672, L103
Kennicutt, R. C., Jr., Tamblyn, P., & Congdon, C. E. 1994, ApJ, 435, 22
Kovac, K., et al. 2009, arXiv:0909.2032
Lewis, I., et al. 2002, MNRAS, 334, 673
Liu, C. T., & Kennicutt, R. C., Jr. 1995, ApJ, 450, 547
Mahajan, S., & Raychaudhury, S. 2009, MNRAS, 400, 687
Marcillac, D., Rigby, J. R., Rieke, G. H., & Kelly, D. M. 2007, ApJ, 654, 825
Martini, P., Kelson, D. D., Kim, E., Mulchaey, J. S., & Athey, A. A. 2006, ApJ, 644, 116
McCarthy, I. G., Frenk, C. S., Font, A. S., Lacey, C. G., Bower, R. G., Mitchell, N. L., Balogh, M. L., & Theuns, T. 2008, MNRAS, 383, 593
McGee, S. L., Balogh, M. L., Bower, R. G., Font, A. S., & McCarthy, I. G. 2009, MNRAS, 400, 937
Merchán, M., & Zandivarez, A. 2002, MNRAS, 335, 216
Mihos, J. C., & Hernquist, L. 1994, ApJ, 431, L9
Miles, T. A., Raychaudhury, S., Forbes, D. A., Goudfrooij, P., Ponman, T. J., & Kozhurina-Platais, V. 2004, MNRAS, 355, 785
Mulchaey, J. S., & Zabludoff, A. I. 1998, ApJ, 496, 73
Noeske, K. G., et al. 2007, ApJ, 660, L43
Rasmussen, J., Mulchaey, J. S., Bai, L., Ponman, T. J., Raychaudhury, S., & Darish, A. 2010, ApJ, submitted
Rasmussen, J., Ponman, T. J., & Mulchaey, J. S. 2006a, MNRAS, 370, 453
Rasmussen, J., Ponman, T. J., Mulchaey, J. S., Miles, T. A., & Raychaudhury, S. 2006b, MNRAS, 373, 653
Rieke, G. H., Alonso-Herrero, A., Weiner, B. J., Pérez-González, P. G., Blaylock, M., Donley, J. L., & Marcillac, D. 2009, ApJ, 692, 556
Rieke, G. H., et al. 2004, ApJS, 154, 25
Saintonge, A., Tran, K.-V. H., & Holden, B. P. 2008, ApJ, 685, L113
Salim, S., et al. 2007, ApJS, 173, 267
Salim, S., et al. 2009, ApJ, 700, 161
Schlegel, D. J., Finkbeiner, D. P., & Davis, M. 1998, ApJ, 500, 525
Shen, Y., Mulchaey, J. S., Raychaudhury, S., Rasmussen, J., & Ponman, T. J. 2007, ApJ, 654, L115
Strateva, I., et al. 2001, AJ, 122, 1861
Temi, P., Brighenti, F., & Mathews, W. G. 2009a, ApJ, 695, 1
Temi, P., Brighenti, F., & Mathews, W. G. 2009b, ApJ, 707, 890
Tran, K.-V. H., Saintonge, A., Moustakas, J., Bai, L., Gonzalez, A. H., Holden, B. P., Zaritsky, D., & Kautsch, S. J. 2009, ApJ, 705, 809
Tully, R. B. 1987, ApJ, 321, 280
Vulcani, B., Poggianti, B. M., Finn, R. A., Rudnick, G., Desai, V., & Bamford, S. 2010, ApJ, 710, L1
Weinmann, S. M., van den Bosch, F. C., Yang, X., & Mo, H. J. 2006, MNRAS, 366, 2
Wilman, D. J., Balogh, M. L., Bower, R. G., Mulchaey, J. S., Oemler, A., Carlberg, R. G., Morris, S. L., & Whitaker, R. J. 2005, MNRAS, 358, 71
Wolf, C., et al. 2009, MNRAS, 393, 1302
Yang, X., Mo, H. J., van den Bosch, F. C., & Jing, Y. P. 2005, MNRAS, 356, 1293
Zabludoff, A. I., & Mulchaey, J. S. 1998, ApJ, 496, 39